III. 研究成果の刊行に関する一覧

研究成果の刊行に関する一覧表
【H25. 4. 1～H26. 3. 31】

雑誌

発表者氏名	論文タイトル名	発表誌名	巻号	ページ	出版年
Asagiri M et al.	Generation of a mouse model with down-regulated U50 snoRNA (SNORD50) expression and its organ-specific phenotypic modulation. PLoS One. 2013;8(8):e72105.	PLoS One	8	E72105	2013
Asagiri M, Uemoto S, Iwaisako K et al.	Cilostazol attenuates hepatic stellate cell activation and protects mice against carbon tetrachloride-induced liver fibrosis.	Hepatol Res.	44	460-473	2014
Uemoto S, Iwaisako K et al.	Whey-hydrolyzed peptide-enriched immunomodulating diet prevents progression of liver cirrhosis in rats.	Nutrition	30	1195-1207.	2014
Uemoto S, Iwaisako K. et al.	Effects of oral intake of hydrogen water on liver fibrogenesis in mice.	Hepatol Res.	44	663-677	2014

IV. 研究成果の刊行物・別刷

OPEN ACCESS Freely available online

PLOS ONE

Generation of a Mouse Model with Down-Regulated U50 snoRNA (SNORD50) Expression and Its Organ-Specific Phenotypic Modulation

Yuuichi Soeno[1]*, Kazuya Fujita[1], Tomoo Kudo[2], Masataka Asagiri[3], Shigeru Kakuta[4,5], Yuji Taya[1], Yoshihito Shimazu[1], Kaori Sato[1], Ritsuko Tanaka-Fujita[6], Sachiko Kubo[5,7], Yoichiro Iwakura[5,7], Yoshikazu Nakamura[8,9], Shigeo Mori[10], Takaaki Aoba[1]

1 Department of Pathology, School of Life Dentistry, The Nippon Dental University, Tokyo, Japan, **2** Department of Pathology, Hyogo College of Medicine, Hyogo, Japan, **3** Innovation Center for Immunoregulation and Therapeutics, Graduate School of Medicine, Kyoto University, Kyoto, Japan, **4** Department of Biomedical Science, Graduate School of Agricultural and Life Sciences, University of Tokyo, Tokyo, Japan, **5** Center for Experimental Medicine and Systems Biology, Institute of Medical Science, University of Tokyo, Tokyo, Japan, **6** Risk Assessment Division, Food Safety Commission Secretariat, Cabinet Office, Government of Japan, Tokyo, Japan, **7** Division of Experimental Animal Immunology, Research Institute for Biomedical Sciences, Tokyo University of Science, Chiba, Japan, **8** Division of RNA Medical Science, Institute of Medical Science, University of Tokyo, Tokyo, Japan, **9** Ribomic Inc., Tokyo, Japan, **10** Kotobiken Medical Laboratories Inc., Tokyo, Japan

Abstract

Box C/D-type small nucleolar RNAs (snoRNAs) are functional RNAs responsible for mediating 2′-*O*-ribose methylation of ribosomal RNAs (rRNAs) within the nucleolus. In the past years, evidence for the involvement of human U50 snoRNA in tumorigenesis has been accumulating. We previously identified *U50HG*, a non-protein-coding gene that hosted a box C/D-type U50 snoRNA, in a chromosomal breakpoint in a human B-cell lymphoma. Mouse genome analysis revealed four mouse U50 (mU50) host-genes: three *mU50HG-a* gene variants that were clustered in the genome and an *mU50HG-b* gene that we supposed to be the *U50HG* ortholog. In this study, to investigate the physiological importance of mU50 snoRNA and its involvement in tumorigenesis, we eliminated mU50 snoRNA sequences from the *mU50HG-b* gene. The established mouse line ($\Delta mU50_{(HG\text{-}b)}$) showed a significant reduction of mU50 snoRNA expression without alteration of the host-gene length and exon-intron structure, and the corresponding target rRNA methylation in various organs was reduced. Lifelong phenotypic monitoring showed that the $\Delta mU50_{(HG\text{-}b)}$ mice looked almost normal without accelerated tumorigenicity; however, a notable difference was the propensity for anomalies in the lymphoid organs. Transcriptome analysis showed that dozens of genes, including heat shock proteins, were differentially expressed in $\Delta mU50_{(HG\text{-}b)}$ mouse lymphocytes. This unique model of a single snoRNA knockdown with intact host-gene expression revealed further new insights into the discrete transcriptional regulation of multiple mU50 host-genes and the complicated dynamics involved in organ-specific processing and maintenance of snoRNAs.

Citation: Soeno Y, Fujita K, Kudo T, Asagiri M, Kakuta S, et al. (2013) Generation of a Mouse Model with Down-Regulated U50 snoRNA (SNORD50) Expression and Its Organ-Specific Phenotypic Modulation. PLoS ONE 8(8): e72105. doi:10.1371/journal.pone.0072105

Editor: Jürgen Brosius, University of Münster, Germany

Received February 26, 2013; **Accepted** July 7, 2013; **Published** August 26, 2013

Funding: This work was supported by Grants-in-Aid for Scientific Research from the Ministry of Education, Science and Culture of Japan #20791374 (http://www.mext.go.jp/). The funders had no role in study design, data collection and analysis, decision to publish, or preparation of the manuscript.

Competing Interests: Authors Yoshikazu Nakamura and Shigeo Mori are employed by Ribomic Inc. and Kotobiken Medical Laboratories Inc., respectively. This does not alter the authors' adherence to all the PLOS ONE policies on sharing data and materials.

* E-mail: soeno-path@tky.ndu.ac.jp

Introduction

Small nucleolar RNAs (snoRNAs) are one of the abundant non-protein-coding RNA species (>300 snoRNAs have been found in human) that are responsible for the maturation of ribosomal RNAs (rRNAs) within the nucleolus [1,2]. snoRNAs achieve site-specific nucleotide modification by base-pairing to complementary sequences on rRNA precursors. Based on the conserved nucleotide sequences and their function, snoRNAs are grouped into two classes: box C/D-type snoRNAs and box H/ACA-type snoRNAs that catalyze 2′-*O*-ribose methylation and pseudouridylation, respectively [3–6]. Eukaryotic snoRNA genes are commonly harbored in introns of their host-genes, and snoRNA expression is coupled with splicing of the host-gene pre-mRNA [7–9], although some H/ACA-type snoRNAs have alternative routes of maturation [10]. Most snoRNA host-genes encode proteins that play a role in the translation machinery of cells. On the other hand, there are several snoRNA host-genes that do not encode proteins but instead possess a 5′-terminal oligopyrimidine (5′TOP) motif that is reminiscent of the signal sequence of ribosomal protein genes [11–13]. With respect to the physiological roles of snoRNAs, loss-of-function studies for a single snoRNA in yeast have so far demonstrated that the snoRNA-assisted rRNA modifications were not critical but, in part, caused subtle phenotypic alterations in cell growth [14,15]. However, molecular genetic approaches have rarely been used to explore the physiological and pathogenetic importance of individual snoRNAs in higher organisms [16].

In a previous investigation of a novel translocation partner of *BCL6* at t(3;6)(q27;q15) in a human diffuse large B-cell lymphoma, we found a snoRNA host-gene, *U50HG*, that encoded U50

snoRNA within its intron [17] (*U50HG* and U50 snoRNA are now named *SNHG5* and *SNORD50*, respectively). U50 snoRNA belongs to the box C/D snoRNA class and has two regions in its sequence that are complementary to the human 28S rRNA [3,4]. The U50 snoRNA is highly expressed in hematopoietic and lymphoid organs such as thymus, spleen, bone marrow, and lymph nodes [17]. *U50HG* has been identified as a non-protein-coding host-gene with a 5′TOP motif. Regarding the involvement of U50 snoRNA in human tumorigenicity, recent studies have reported that a genomic mutation in the U50 snoRNA gene (deletion of two thymidine residues in the middle of the gene) was related to poor prognosis in cancer patients [18,19]. It has also been reported that over-expression of U50 snoRNA inhibited colony formation of human prostate cancer and breast cancer cell lines *in vitro*, suggesting that U50 snoRNA may behave as a tumor suppressor [18,19]. At present, although details of the organ-specific regulation of *U50HG* and U50 snoRNA expression still remain elusive, it is an intriguing hypothesis that the perturbation of U50 snoRNA alone or coupled with an anomalous host-gene function might evoke causative or additive effects on tumorigenesis in an organ-specific manner.

During a genomic search for U50-related genes in mice, we previously identified a mouse U50 (mU50) snoRNA and the two 5′TOP non-protein-coding host-genes, *mU50HG-a* and *mU50HG-b* on mouse chromosome 9E3-F1 (syntenic with human 6q15 where *U50HG* is located) [20]. In that report, we proposed that *mU50HG-b* might be an ortholog to the human *U50HG* gene because of the structural similarity between the two genes and that *mU50HG-a* was presumably duplicated from *mU50HG-b* in mouse [20].

Based on these findings, we have generated a novel mouse model in which the expression of *mU50HG-b*-derived mU50 snoRNA is depleted without altering the host-gene length and genomic structure. Using this mouse model, it should be possible to investigate the physiological roles of the single snoRNA independent of the effect of the host-gene function. We found that the deletion of *mU50HG-b*-encoded mU50 snoRNA sequences resulted in a marked reduction in the quantity of mU50 snoRNA and methylation of the target rRNA, and that the perturbation of mU50 snoRNA was not crucial for growth and lifespan but yielded subtle anomalies and gene modulation in the lymphoid organs.

Results

Generation of ΔmU50$_{(HG\text{-}b)}$ Mice and their Phenotype

To generate a U50 snoRNA deficient mouse model, we reinvestigated the genomic loci of mU50 host-genes in the C57BL/6 mouse genome in the NCBI database (http://www.ncbi.nlm.nih.gov/genome/). We found a *mU50HG-b* gene and a cluster of three distinct *mU50HG-a* gene structures (*mU50HG-a(1)*, *-a(2)*, and *-a(3)*) annotated on chromosome 9 (Fig. 1A). Sequence alignment of the host-genes and the corresponding transcripts revealed that *mU50HG-a(2)* was the 5′TOP *mU50HG-a* gene that we had reported previously [20]. In addition, when each of the intron-encoded mU50 snoRNA sequences in the *mU50HG-a* host-genes were compared, we found three single nucleotide polymorphisms in the middle of the snoRNA sequences that did not correspond to the complementary sequence to the rRNA target. We designated these mU50 snoRNA variants mU50_v1, mU50_v2, and mU50_v3 according to the host-gene name (Fig. 1B). *mU50HG-b* harbored two of these variants, mU50_v1 and mU50_v2, within the introns. Computer-assisted prediction of the RNA structures (MFold; http://mfold.rna.albany.edu/) revealed that these mU50 snoRNA sequence variants formed identical secondary structures in their most stable energy state (Fig. S1A). The sequences of the two antisense elements in mU50 snoRNA that interact with the target rRNA were conserved in the three mU50 snoRNA variants as well as in human U50 snoRNA (Fig. S1B).

Gene targeting successfully generated heterozygous mice that possessed a mutant allele in which two mU50 snoRNA sequences located within the introns of the *mU50HG-b* gene were completely replaced by external sequences (Fig. 2A). The neomycin-resistant gene (1.7 kbp) was removed out by cross-breeding the heterozygous mice with CAG-Cre mice [21] in which Cre recombinase, which catalyzes recombination between two loxP sites, was expressed (Fig. 2B). The overall length and exon-intron structure of the reconstructed *mU50HG-b* gene were identical to those of the wild-type *mU50HG-b* (Fig. S2). By breeding the heterozygotes, we obtained homozygous mice that had a pair of the mutant alleles inherited maternally and paternally. A newly generated recognition site for the *Eco*RV restriction enzyme in the reconstructed *mU50HG-b* allowed the genotypes to be distinguished by PCR amplification followed by digestion of the PCR product with *Eco*RV (Fig. 2C). The mutant mice were born at Mendelian ratios and the ratio of female over male of 0.49 was comparable to the ratio of 0.48 found in the wild-type mice. We designated the mutant homozygotes as ΔmU50$_{(HG\text{-}b)}$ mice. In the homozygous mating (n = 30), the average number of littermates was 5.9, similar to the 6.0 for the wild-type mice. The ΔmU50$_{(HG\text{-}b)}$ mice appeared to grow normally, and were able to become pregnant, give birth, and feed their offspring.

Phenotypic characteristics of ΔmU50$_{(HG\text{-}b)}$ mice, namely weight gain, wet weights of various organs, and peripheral blood chemistry and cytology were similar to those of wild-type (Figs. S3A–S3C). No significant difference in the cell proliferation activity was observed when the splenocytes isolated from the individual genotypes were grown in an *in vitro* culture system (Fig. S3D). In our lifelong monitoring of the health condition of the mice, we encountered a greater number of splenomegaly (an enlargement of the spleen) and swollen lymph nodes in the population of ΔmU50$_{(HG\text{-}b)}$ mice when age-matched populations of both genotypes (from 35 to 98 weeks-old; n = 40 per genotype; Fisher's exact test, $P = 0.0482$) were compared (Fig. 2D). However, no difference in tumor development was observed in both genotypes (Table S1).

Expression of mU50 snoRNAs and mU50 Host-genes in ΔmU50$_{(HG\text{-}b)}$ Mice

Northern blot analysis showed that, when compared with the age-matched wild-type mice, the intensity of the mU50 snoRNA signal was reduced markedly in all organs (i.e., brain, lung, heart, liver, pancreas, kidney, spleen, and lymph nodes) analyzed in 10-week-old ΔmU50$_{(HG\text{-}b)}$ mice (Fig. 3A). The oligonucleotide probe that was used targets a region of mU50 snoRNA that is completely conserved in all three mU50 snoRNA variants as well as in human U50 snoRNA (Fig. 1B). It is notable that the mU50 snoRNA signals in wild-type mice were most prominent in the lymphoid organs (spleen and lymph nodes) (Fig. 3A, right). A comparison of the mU50 snoRNA signals in the spleen of wild-type, ΔmU50$_{(HG\text{-}b)}$-homozygous and heterozygous mice showed that the mU50 snoRNA signal was reduced by half in heterozygous mice, but no difference was found between mice with either the maternally (−/+) or paternally (+/−) inherited mutant allele (Fig. 3B). We also confirmed that the mU50 snoRNA-deficient condition was maintained in the corresponding organs in 60-week-old ΔmU50$_{(HG\text{-}b)}$ mice (data not shown).

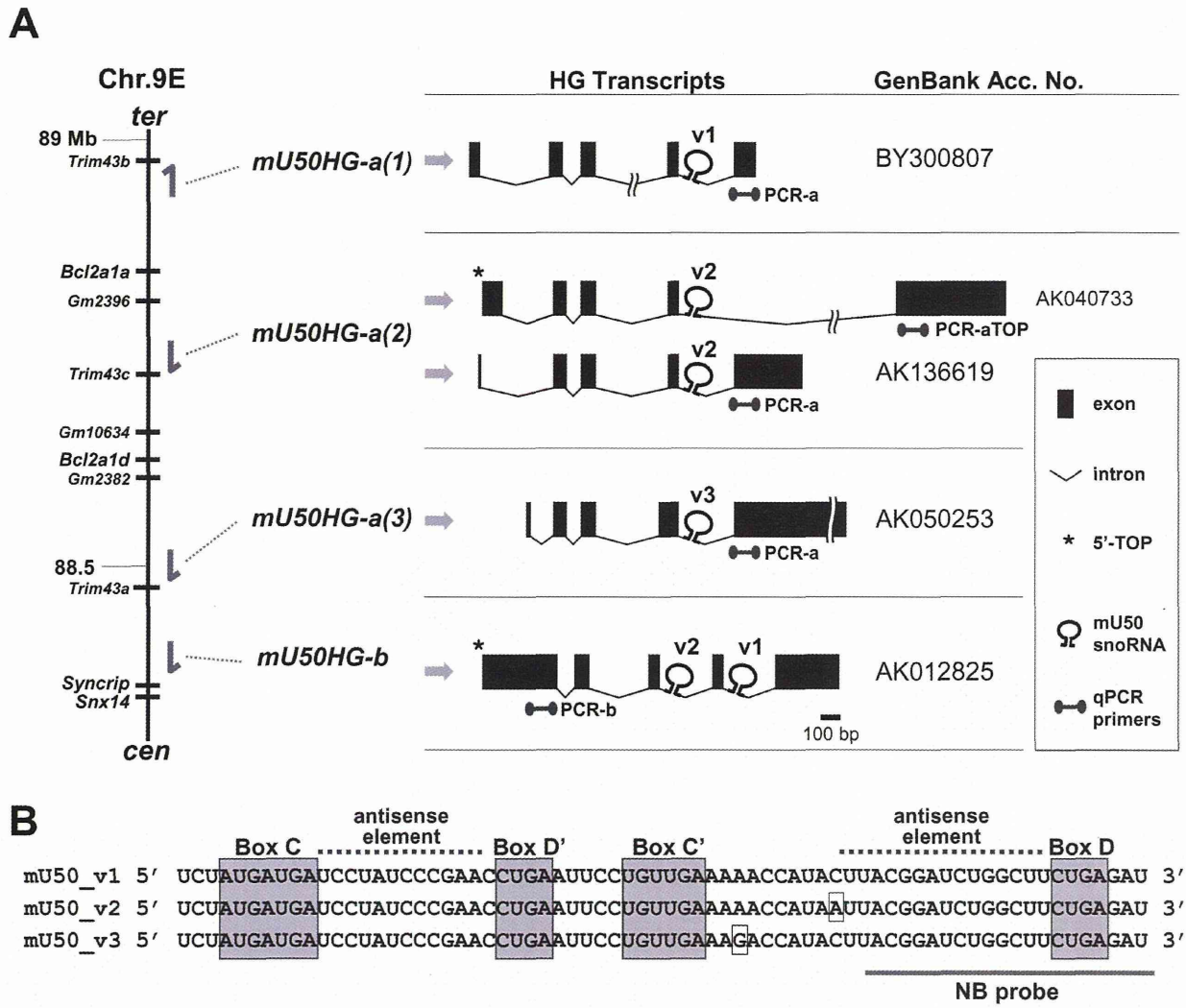

Figure 1. Genomic structure of mU50 host-genes on mouse chromosome 9. (A) Structure of transcripts for the mouse mU50 host-genes. Three *mU50HG-a*, *mU50HG-a(1)*, *-a(2)* and *-a(3)*, and the *mU50HG-b* loci are indicated sequentially by the arrows from the terminus (ter) to the centromere (cen) on the mouse chromosome. The mU50 host-genes except for *mU50HG-a(1)* are encoded in antisense direction. The right column illustrates the corresponding host-gene transcripts and their intron-encoded mU50 snoRNA variants, v1, v2, and v3. *mU50HG-b* contains mU50_v1 and v2 in distinct introns. Note that *mU50HG-a(2)* provides alternative splice variants. One transcript (AK040733) has a 5′TOP sequence (shown by asterisk) at the first exon, regarding our previous finding of the 5′TOP *mU50HG-a* gene [20]. The other splice variant (AK136619) possess the same sequence region at the fifth exon as the *mU50HG-a(1)* and *-a(3)*. We do not show an additional splice variant of *mU50HG-a(2)* (AK007093) listed in the GenBank database because the nucleotide length of the mU50-containing intron (17 kb) exceeds the appropriate length required for efficient processing of C/D-type snoRNA (≈85 nucleotides [45]). The primer sets used in qPCR analyses (Fig. 4) are also indicated. (B) Sequence of the mU50 variants, v1, v2 and v3. Conserved box sequences (C, D′, C′, and D) are indicated by gray rectangles. Two antisense elements, where the mU50 snoRNA interacts with the target rRNA, are indicated by broken lines. The single nucleotide polymorphisms among the variants are also shown by rectangles. NB: Northern blot.
doi:10.1371/journal.pone.0072105.g001

As illustrated in Fig. 1A, the mU50 host-genes, *mU50HG-a(1)*, *-a(2)*, and *-a(3)*, encode each of the discrete mU50 snoRNA variants, namely, mU50_v1, mU50_v2, and mU50_v3, respectively, while the *mU50HG-b* host-gene encodes two mU50 sequences that correspond to the mU50_v1 and mU50_v2 snoRNAs. We found that the abundant expression of the *mU50HG-b*-derived mU50_v1 and v2 snoRNAs was eliminated in ΔmU50$_{(HG\text{-}b)}$ mice and, therefore, sought to clarify the distribution of the mU50 snoRNA variants that were expressed from the *mU50HG-a* genes among the various organs in the ΔmU50$_{(HG\text{-}b)}$ mice using PCR-SSCP (single-strand conformation polymorphism). Analysis of the genomic DNA extracted from ΔmU50$_{(HG\text{-}b)}$ mouse embryos supported the presence of single copies of each of the *mU50HG-a* gene variants (Fig. 3C, the first lane). In addition, we found that the proportion of the mU50 snoRNA variant-derived signals varied in individual organs (Fig. 3C): mU50_v2 was predominant in lung and spleen; both mU50_v1 and mU50_v2 were predominant in brain and heart; and all three variants were evenly expressed in liver and kidney. This finding indicates that the *mU50HG-a*-derived mU50 snoRNA

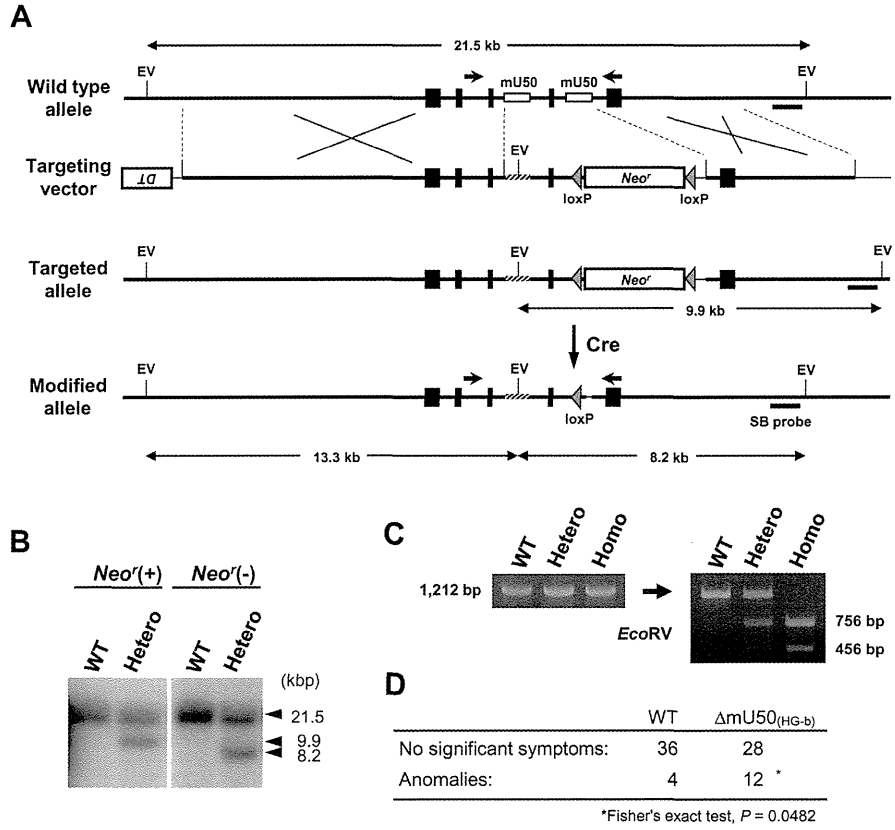

Figure 2. Generation of the mU50-deficient mice. (A) Schematic representation of the targeting strategy based on the wild-type allele. In the targeting vector, the first mU50 snoRNA sequence (upstream) is substituted by the 68 bp multiple cloning site of a pBluescriptII KSII plasmid containing an *Eco*RV recognition site (EV). The second mU50 snoRNA sequence (downstream) is replaced with a loxP-*Neo*^{r}-loxP cassette. The pair of facing arrows indicates the set of forward/reverse primers used for genotyping PCR. *DT*: diphtheria toxin negative selection cassette; *Neo*^{r}: neomycin resistant gene cassette; *Cre*: treatment with Cre recombinase; *SB probe*: a probe for Southern blot. (B) Southern blot of genomic DNA from mutant heterozygotes before (left) and after (right) removal of the *Neo*^{r} cassette by Cre recombinase. WT: wild-type; Hetero: mutant heterozygotes. (C) Genotyping PCR for the *mU50HG-b* gene. Note that all the PCR products had nucleotide lengths that were identical to that of the wild-type. After digestion of the PCR product with *Eco*RV, fragmentation of the mutant allele-derived amplicon was observed. WT: wild-type; Hetero: mutant heterozygotes; Homo: $\Delta mU50_{(HG\text{-}b)}$ mutant. (D) Lifelong monitoring of the health condition (n = 40 per genotype) of $\Delta mU50_{(HG\text{-}b)}$ and wild-type mice. Note the greater number of anomalies in the $\Delta mU50_{(HG\text{-}b)}$ population. Detailed list is available in Table S1.
doi:10.1371/journal.pone.0072105.g002

variants also showed organ-specific expression patterns, although the organ specificities for the *mU50HG-a*-derived variants were different from those elucidated for the *mU50HG-b*-derived snoRNAs.

To analyze the expression levels of the mU50 host-genes by quantitative PCR (qPCR), we designed three sets of primers to differentially detect *mU50HG-b*, *mU50HG-a* (all three gene variants), and a 5′TOP transcript of *mU50HG-a(2)* (Fig. 1A). In wild-type mice, the substantial expression of *mU50HG-b* was observed in the all organs analyzed; the expression levels were higher in brain, lung, heart, liver, and spleen, and lower in pancreas, kidney, and lymph nodes (Fig. 4, top). Regarding the expression levels of the *mU50HG-a* variants, the use of two primer sets yielded comparable results: the highest level in heart and lower levels in all the other organs analyzed (Fig. 4, middle and bottom). In $\Delta mU50_{(HG\text{-}b)}$ mice, it is notable that *mU50HG-b* expression increased significantly in the lymphoid organs, whereas the corresponding host-gene expression in the other organs was comparable to their expression in the wild-type mice (Fig. 4, top). The expression profiles of *mU50HG-a* host-genes in $\Delta mU50_{(HG\text{-}b)}$ mice were similar to those in wild-type mice (middle), but the expression of the 5′TOP transcript of *mU50HG-a(2)* increased significantly in both spleen and lymph node of $\Delta mU50_{(HG\text{-}b)}$ mice compared with in wild-type, as was observed for the 5′TOP *mU50HG-b* transcript (Fig. 4, bottom).

Influence of *mU50HG-b*-derived mU50 snoRNA Depletion on Cellular Function in $\Delta mU50_{(HG\text{-}b)}$ Mice

To evaluate whether the reduced amount of mU50 snoRNA affected methylation status of the target rRNA in the cells, a primer extension assay was performed for mU50 snoRNA-target sites on 28S rRNA (Fig. 5A). In this assay, a deoxynucleotide concentration as low as 0.004 mM made the reverse transcriptase methylation-sensitive and this resulted in the cessation of polymerization one nucleotide before a methylated nucleotide. We found that the resulting stop signals on the 28S rRNA (Cm2613 and Gm2628) were largely eliminated in all the studied organs of the $\Delta mU50_{(HG\text{-}b)}$ mice, showing that the box C/D mU50 snoRNAs caused the loss of canonical rRNA modification (Fig. 5B).

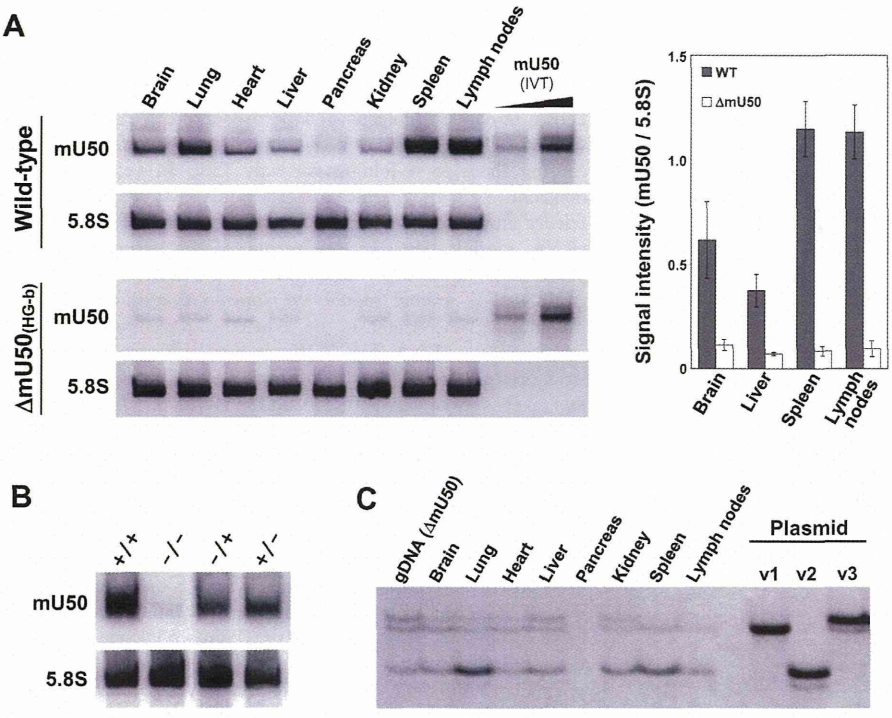

Figure 3. Molecular aspects of different organs in $\Delta mU50_{(HG\text{-}b)}$ and wild-type mice. (A) Northern blot analysis of mU50 snoRNA expression in eight organs from wild-type and $\Delta mU50_{(HG\text{-}b)}$ mice. *In vitro* transcribed (IVT) mU50 snoRNA was applied as a control. Detection of 5.8S rRNA was performed for the loading control. The signal intensities of selected organs are indicated in the panel on the right of the Figure. (B) Northern blot analysis of mU50 snoRNA and 5.8S rRNA expression in spleen obtained from wild-type (+/+), $\Delta mU50_{(HG\text{-}b)}$ (−/−), and maternally (−/+) and paternally (+/−)-inherited $\Delta mU50_{(HG\text{-}b)}$ heterozygotes. (C) PCR-SSCP analysis of the mU50 snoRNA variants in $\Delta mU50_{(HG\text{-}b)}$ mice. Genomic DNA from $\Delta mU50_{(HG\text{-}b)}$ mouse, which contains a single copy of each *mU50HG-a* paralog, was used as the control PCR template. gDNA: genomic DNA; v1, v2 and v3: plasmids that correspond to the mU50 snoRNAs encoded by *mU50HG-a(1)*, *-a(2)*, and *-a(3)*, respectively.
doi:10.1371/journal.pone.0072105.g003

To assess the influence of reduced mU50 snoRNA status on the overall gene expression profile, we conducted a microarray-based analysis using isolated splenic B-lymphocytes (Table 1). We found 42 genes that were differentially expressed (>1.5-fold) between the wild-type and $\Delta mU50_{(HG\text{-}b)}$ mice, including immunoglobulin (Ig) genes and several heat shock protein (Hsp) family genes. The qPCR analysis validated the significant up-regulation of X-linked lymphocyte-regulated 3A (*Xlr3a*) and dual von Willebrand factor A (*Dvwa*; also known as collagen VI alpha 4 gene *Col6a4*) in $\Delta mU50_{(HG\text{-}b)}$ splenic B-lymphocytes (Fig. 6). Notably, *Xlr3a* was up-regulated in spleen and lymph nodes in $\Delta mU50_{(HG\text{-}b)}$ mice, while it remained stable or was down-regulated in the other organs analyzed (Fig. 6A). *Dvwa* was also up-regulated in spleen, but not in lymph nodes, in $\Delta mU50_{(HG\text{-}b)}$ mice (Fig. 6B). In a preliminary 2D electrophoresis in combination with peptide mass fingerprinting analysis, the only differentially expressed proteins that were detected were peptides derived from Hsp70 and an actin-like unnamed protein product (data not shown). Gene expression analysis also showed that *c-Myc*, a possible transcriptional regulator of human *U50HG* gene [22], and *Bcl6*, a transcriptional repressor in relation to translocation in human lymphoma [17], were detected at similar expression levels in the wild-type and $\Delta mU50_{(HG\text{-}b)}$ mice (Fig. S4).

Discussion

We have successfully generated a mouse line that shows significant reduction of mU50 snoRNA expression without modification of the host-gene structure (Fig. 2 and 3A). In previous studies, snoRNA-knockout mouse models were established in relation to the etiology of a human neurodegenerative disorder, Prader-Willi syndrome [23,24]. In these mouse models, more than 40 copies of intron-encoded box C/D-type snoRNA, SNORD116 (formerly HBII-85), and exons of the non-coding host-gene were removed by targeted deletion of a huge genomic locus (≈150 kb). In this respect, the $\Delta mU50_{(HG\text{-}b)}$ mouse generated in this study is the first model in which a single methylation-guide snoRNA is eliminated without altering the genomic structure of the host-gene.

Reduction of mU50 snoRNA Caused by Gene-deletion was not Causative for Tumorigenicity but was Responsible for Alterations in the Lymphoid Organs

The lifelong monitoring of age-matched genotypes showed no marked alterations in phenotypic characteristics of $\Delta mU50_{(HG\text{-}b)}$ mice, such as weight gain, wet weights of various organs, and cell proliferation activity in an *in vitro* culture system (Fig. S3). There was no genotype-related difference in the incidence of tumor development in the whole body but, in connection with the abundant mU50 snoRNA expression in the lymphoid organs in wild-type mice, splenomegaly and swollen lymph nodes were observed more frequently in $\Delta mU50_{(HG\text{-}b)}$ mice (Fig. 2D and Table S1).

Our microarray and qPCR analysis revealed altered expression levels of some genes, for example, *Xlr3a* and *Dvwa*, in

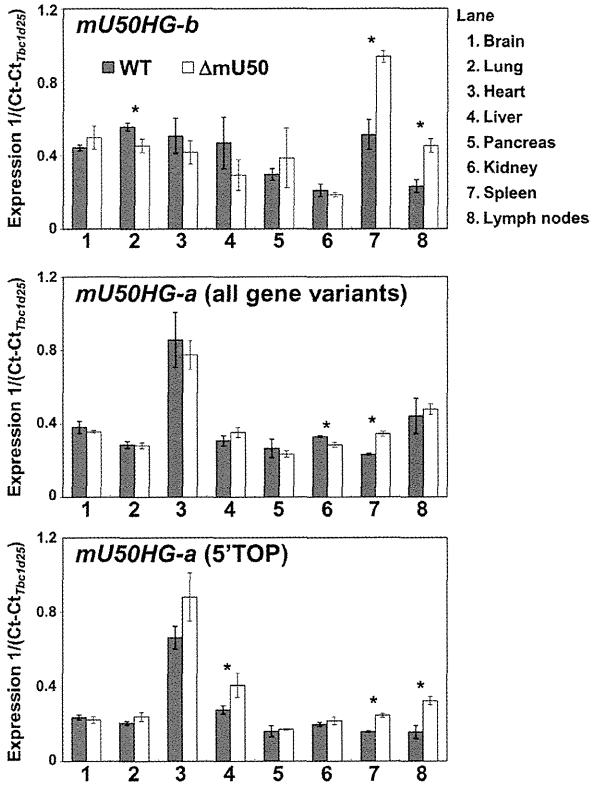

Figure 4. Expression profiles of mU50 host-genes in eight organs from wild-type and ΔmU50$_{(HG-b)}$ mice. Real-time qPCR for determination of the discrete mU50 host-genes were conducted using three primer sets: PCR-b primer set for detection of *mU50HG-b* transcript, PCR-a primer set for amplification of all transcripts from the three *mU50HG-a* loci, and PCR-aTOP primer set for *mU50HG-a(2)* with 5′TOP sequence (see Fig.1A). The threshold value was normalized using the reference gene (*Tbc1d25*). See Materials and methods on the selection of reference genes for mouse organs. Error bars = 1 S.D. for three biological replicates. *$P<0.05$; WT: wild-type; ΔmU50: ΔmU50$_{(HG-b)}$ mice.
doi:10.1371/journal.pone.0072105.g004

ΔmU50$_{(HG-b)}$ B-lymphocytes (Table 1 and Fig. 6). The expression of the *XLR* (X-linked lymphocyte-regulated) gene family is highly correlated with characteristics of a mature phenotype in B-lymphocytes [25]. Mouse *Dvwa* was recently cloned as an equivalent to a collagen type VI gene *Col6a4*, and RT-PCR analysis in adult mice showed the *Dvwa* was highly expressed in ovary, intestine, and spleen [26]. Our qPCR analysis showed that both *Xlr3a* and *Dvwa* were up-regulated markedly in ΔmU50$_{(HG-b)}$ spleen, whereas their expression levels in the other ΔmU50$_{(HG-b)}$ organs analyzed were either unaffected or down-regulated (Fig. 6). Regarding the putative interaction between mU50 snoRNA and gene transcripts, it is notable that both *Xlr3a* and *Dvwa* mRNAs contain multiple sequences (≈12 nucleotides) that are complementary to the mU50 snoRNA (data not shown). Other studies have suggested multiple roles of snoRNAs in post-transcriptional events such as alternative splicing, A-to-I RNA editing, and RNA chaperone activity, in addition to their modification-guidance role [27–29]). Whether mU50 snoRNAs contribute to the post-transcriptional regulation of these genes still needs to be explored; however, our findings coupled with the abundant mU50 snoRNAs support the possible functional importance of mU50 snoRNA in lymphoid organ physiology.

Gene expression profiling showed that genes encoding Hsp were up-regulated in ΔmU50$_{(HG-b)}$ mice (Table 1). The Hsp family is known to contain molecular chaperones that are expressed under various cellular stresses and they interact with misfolded proteins causing them to re-folding correctly [30]. In yeast, ribosomes deficient in rRNA modifications succumb to altered translational fidelity supporting the proposed importance of snoRNA-mediated rRNA modifications in optimizing rRNA structure for the production of accurate and efficient ribosomes [31]. In our ΔmU50$_{(HG-b)}$ animal model, we showed that the depletion of mU50 snoRNA resulted in the reduced methylation status of the corresponding rRNA (Fig. 5). By extrapolating from the tertiary structure of *Thermus thermophilus* ribosomes [32], we found that the two target sites of U50 snoRNA on the rRNA (U50-sites; identical in both human and mouse) were located at the inter-subunit bridge of 23S rRNA (corresponding to 28S rRNA in vertebrates) (Fig. S1C). The inter-subunit bridge is responsible for the attachment between the large and small ribosomal subunits and is distant from the peptidyl transferase center that is a core region for the ribozyme activity of ribosomes [33]. We postulate that the U50-sites are not critical for protein synthesis but that they might disturb the harmonic motion between ribosomal subunits, leading to perturbations in protein synthesis. From a phylogenetic point of view, it is of interest that the corresponding U50-sites in rRNAs are highly conserved through bacteria to vertebrates (Fig. S1C), but no methylation occurs at the corresponding sites in bacteria and yeast because of a lack of orthologous U50 snoRNA in these non-vertebrate classes [34]. Taken together, we hypothesize that U50 snoRNA-mediated methylation might be relatively newly required in vertebrates, and it may be particular important in fine-tuning regulation of the hematopoietic system and lymphoid function concomitant with the development of acquired immunity. In this context, we speculate that the ribosomes in lymphoid organs need a higher amount of mU50 snoRNA for the abundant production of immunoglobulin, and therefore, upon substantial reduction in mU50 snoRNA in our ΔmU50$_{(HG-b)}$ model, the proteins that are translated by the modified ribosomes might require a chaperone machinery that is supported by the induced Hsp proteins.

Differential Expression Patterns of mU50 Host-genes and mU50 snoRNA among Different Organs

The results of mU50 host-gene expression obtained by qPCR revealed that together the mU50 host-genes represent a substantial amount of the transcripts in all the organs analyzed in both wild-type and ΔmU50$_{(HG-b)}$ mice (Fig. 4). Of most interest was the organ-dependency of *mU50HG-b* expression, for example, higher in heart and liver and lower in lymph nodes, which is inconsistent with the organ-specific distribution of mU50 snoRNA, for example, their enrichment in spleen and lymph nodes and their sparseness in heart and liver (Fig. 3A). In general, the processing of non-protein-coding host-gene transcripts are identified and rapidly degraded in cells by nonsense-mediated decay (NMD) [35], although it has also been documented that snoRNA host-gene transcripts display variable susceptibility to NMD [36]. Thus, a possible scenario is that the mU50 host-gene transcripts are particularly susceptible to NMD in some organs, as has been shown for the *U87HG* transcript [36]; alternatively, the mU50 snoRNAs in non-lymphoid organs might be eliminated rapidly by RNA degradation machinery. Regarding RNA degradation, recent studies using deep sequencing provided evidence that snoRNA products are processed by RNA degradation machinery,

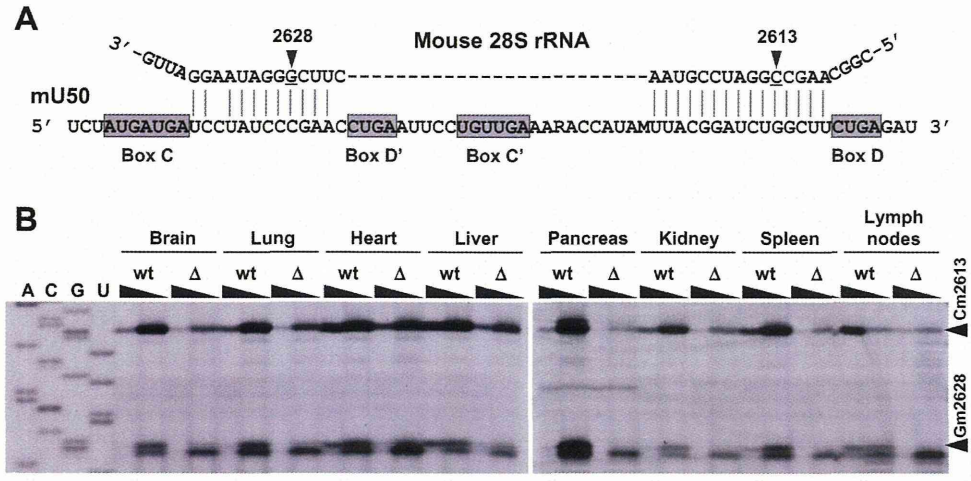

Figure 5. Mechanism of action of mU50 snoRNA. (A) Schematic representation of mU50 snoRNA binding to 28S rRNA. The mU50 snoRNA sequence contains two sites that are complementary to two methylation-target sites in the 28S rRNA sequence. Consensus C and D (and C′ and D′) box motifs are shown in shaded rectangles. The ribonucleotides that are located 5 bases prior to boxes D and D′ (indicated by the arrows) are methylated. (B) Methylation-sensitive primer extension assay for U50-sites in various mouse organs. The wedges across every two lanes indicate the concentration of dNTP (1 mM and 0.004 mM) in the reaction mix. The reverse transcriptase generates a stop signal one nucleotide before the 2′-O-methylated nucleotide in the presence of 0.004 mM dNTP. The upper and lower arrows on the right of the Figure indicate the Cm2613 and Gm2628 stop signals on 28S rRNA, respectively. wt: wild-type; Δ: $\Delta mU50_{(HG\text{-}b)}$ mice.
doi:10.1371/journal.pone.0072105.g005

which generates smaller miRNA-like molecules in various types of cells [37–39]. At present, little is known about the degradation machinery for mU50 snoRNA and host-genes in various organs; clearly, further studies are required to elucidate this.

The differential expression profiles of mU50 host-genes imply that mU50 host-genes *per se* may play a role in some organs. Recent studies documented that some non-protein-coding snoRNA host-genes themselves can be active players in cell-cycle regulation. For example, *Gas5* was shown to be involved in the regulation of cell death and proliferation in breast cancer, and its reduced expression was associated with poor prognosis in the studied patients [40]. Cell cycle regulation with the *Gas5* transcript has also been demonstrated in human T-lymphocytes [41]. Another non-protein-coding snoRNA host-gene, *ZFAS1*, which is highly expressed in the human mammary gland, was found to be down-regulated in breast cancer [42]. When the mouse ortholog, *Zfas1*, was down-regulated by siRNA in a mouse mammary cell line, cell proliferation and differentiation were activated without affecting the expression of the snoRNA hosted within its intron [42]. The results obtained from our cell culture experiment indicated that the proliferation activity of $\Delta mU50_{(HG\text{-}b)}$ mice-derived splenocytes was comparable to that of the wild-type splenocytes (Fig. S3D). At this point, we cannot rule out the possibility that mU50 host-genes might have a potential role in cell cycle progression.

U50 snoRNA-releasing Systems in Mouse and Human

Mice possess four mU50 snoRNA-supplying host-genes, three *mU50HG-a* genes and one *mU50HG-b* in their genome, while human have only a single copy of *U50HG* [17]. We previously annotated the *mU50HG-b* gene as a *U50HG* ortholog because of the structural similarity between the two genes. The present reinvestigation of the promoter sequences (from −2,000 to +500 bp flanking the transcription start site) of mU50 host-genes and human *U50HG* further supported the close relationship between *mU50HG-b* and *U50HG* (Fig. S6). In relation to the multiplicity of mU50 host-genes, we initially speculated that *mU50HG-a*-derived mU50 snoRNA might be sufficient to compensate for the depletion of *mU50HG-b*-derived mU50 snoRNA in $\Delta mU50_{(HG\text{-}b)}$ mice. Northern blot analysis, however, indicated that this is not the case; the amount of mU50 snoRNA in $\Delta mU50_{(HG\text{-}b)}$ mice, which should have been derived from the *mU50HG-a* genes, remained very low and did not show a lymphoid organ-specific pattern (Fig. 3A). We also took advantage of the absence of *mU50HG-b*-derived mU50 snoRNAs in $\Delta mU50_{(HG\text{-}b)}$ mice to explore the expression status of *mU50HG-a*-derived mU50 snoRNAs by PCR-SSCP. As a result, we found that the three mU50 snoRNA variants from the three individual *mU50HG-a* genes were differentially expressed among the studied organs but none of them were specific to the lymphoid organs (Fig. 3C). Taking these findings together, we propose that the expression of *mU50HG-b* in mouse, and *U50HG* in human, might contribute uniquely to the enrichment of mU50 snoRNAs in the wild-type lymphoid organs, and the *mU50HG-a* genes in mouse might be regulated independently from *mU50HG-b* expression and may simply have an additional effect on the total amount of mU50 snoRNAs in the corresponding organs. It should be noted that *mU50HG-b* expression was up-regulated in the lymphoid organs of $\Delta mU50_{(HG\text{-}b)}$ mice when mU50 snoRNA expression was substantially reduced (Fig. 4). The observation that the 5′TOP *mU50HG-a* transcript showed similar responses implied that the 5′TOP motif might provide an additional cue for mU50 host-genes to be expressed in the lymphoid organs. Details of the molecular mechanisms that may be involved remain to be explored.

In conclusion, we generated $\Delta mU50_{(HG\text{-}b)}$ mice that lack *mU50HG-b*-derived mU50 snoRNAs in the whole body giving us a unique model of a single snoRNA knockdown with intact genomic host-gene structure and expression. Despite the significant reduction of mU50 snoRNAs and the 2′-*O*-ribose methylation of the target rRNA, the $\Delta mU50_{(HG\text{-}b)}$ mice exhibited normal growth and lifespan. Our major finding is that the influence of mU50 snoRNA depletion, albeit small or mild, appeared mostly in

Table 1. *Differentially expressed genes between wild-type and ΔmU50$_{(HG\text{-}b)}$ mouse B-lymphocytes detected by a comparative microarray analysis.*

Gene Symbol	Gene Title	Ratio	Z-score
Up-regulated in ΔmU50$_{(HG\text{-}b)}$ mice			
*Dvwa**	dual von Willebrand factor A domains	2.56	10.64
Xlr3a	X-linked lymphocyte-regulated 3A	2.63	9.27
Slc15a2	solute carrier family 15 (H+/peptide transporter), member 2	2.24	9.17
Hspa1b	heat shock protein 1B	1.86	7.06
Hsph1	heat shock 105 kDa/110 kDa protein 1	1.77	6.54
Cpt1a	carnitine palmitoyltransferase 1a, liver	1.69	5.98
Siglech	sialic acid binding Ig-like lectin H	1.85	5.91
Mgl1	macrophage galactose N-acetyl-galactosamine specific lectin 1	1.77	5.51
Ddx6	DEAD (Asp-Glu-Ala-Asp) box polypeptide 6	1.53	4.87
Klk1	kallikrein 1	1.65	4.86
Ugcg	UDP-glucose ceramide glucosyltransferase	1.50	4.68
Hspa4l	heat shock protein a4-like	1.60	4.56
Cd209d	CD209d antigen	1.59	4.46
Strn3	striatin, calmodulin binding protein 3 (probed in intron)	1.57	4.37
A230046K03Rik	RIKEN cDNA A230046K03 gene	1.55	4.23
Lifr	leukemia inhibitory factor receptor	1.55	4.21
Slc5a3	solute carrier family 5 (inositol transporters), member 3	1.54	4.18
Hspa1a	heat shock protein 1A	1.70	4.11
2810442I21Rik	RIKEN cDNA 2810442I21 gene	1.69	4.07
Tbc1d8	TBC1 domain family, member 8	1.52	4.06
Rbm25	RNA binding motif protein 25	1.55	3.40
Down-regulated in ΔmU50$_{(HG\text{-}b)}$ mice			
Gm13051	Zinc finger-containing	0.49	−6.68
Fscn1	fascin homolog 1, actin bundling protein	0.49	−5.73
Sdc1	syndecan 1	0.59	−4.89
Chst1	carbohydrate (keratan sulfate Gal-6) sulfotransferase 1	0.60	−4.81
Ly6k	lymphocyte antigen 6 complex, locus K	0.62	−4.52
Idi1	isopentenyl-diphosphate delta isomerase	0.62	−4.52
Lman1	lectin, mannose-binding, 1	0.62	−4.47

*also known as *Col6a4* (collagen, type VI, alpha 4).
Genes that exhibit >1.5-fold up/down-regulation between wild-type and ΔmU50$_{(HG\text{-}b)}$ mice are listed. Probes target to immunoglobulin genes are omitted from the list (see Materials and Methods; complete dataset is available on online GEO database under the accession number GSE41164).
doi:10.1371/journal.pone.0072105.t001

the lymphoid organs where the mU50 snoRNAs are most abundant in the wild-type animals. A comparison of the expression patterns of mU50 snoRNA and host-genes suggests degradation-resistance of mU50 snoRNAs in lymphoid organs. Hence, in the future, it is important to elucidate the discrete transcriptional regulation of the multiple mU50 host-genes as well as the processing and maintenance of the mU50 snoRNAs for a more detailed understanding of their physiological roles in animals.

Materials and Methods

All the procedures in the present study that involved animals were reviewed and approved by the Research Center for Odontology Section of Biological Sciences in the Nippon Dental University, Japan (Permit Number: 10–18). Statistical analysis was performed using the StatView software version 5.0 (SAS Institute Inc., USA).

Targeting Vector Construction and Generation of an mU50-deficient Mouse Line

We performed long-accurate PCRs for the sequences up- and down-stream of the *mU50HG-b* gene using a clone from the RPCI-22 BAC library segment 1 (Roswell Park Cancer Institute, USA). The PCR products were used as homologous arms in the targeting vector. The diphtheria toxin (DT) cassette, loxP sites, and the neomycin resistance gene (*Neo*^{r}) were subcloned from a pBl-lx-Neo-DT vector. E14.1 derived from 129P2/Ola (obtained from Dr. Nobuaki Yoshida, Institute of Medical Science, The University of Tokyo) were electroporated with 25 μg of a linearized mU50 targeting vector per 10^7 cells. Embryonic stem (ES) cells were then plated onto mitomycin C-treated G418-resistant primary mouse embryonic fibroblast cells and selected with G418. Resistant colonies were picked up 6–8 days after selection. Homologous recombination was screened for by PCR and confirmed by Southern blot analysis. Chimeric mice were produced by an

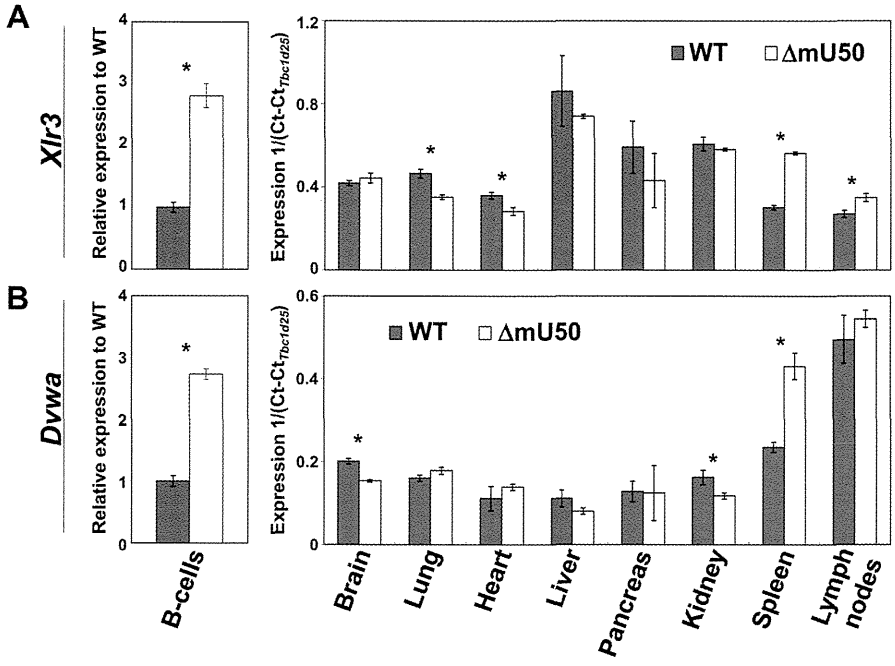

Figure 6. Expression analysis of *Xlr3a* and *Dvwa* genes. TaqMan®-based real-time qPCR was conducted to validate *Xlr3a* (A) and *Dvwa* (B) expression in splenic B-lymphocytes and eight organs. The threshold value was normalized by the reference gene (*Tbc1d25*). Error bars = 1 S.D. for three biological replicates. *$P<0.05$; WT: wild-type; ΔmU50: $\Delta mU50_{(HG\text{-}b)}$ mice.
doi:10.1371/journal.pone.0072105.g006

aggregation method as described previously [43]. Ten to 15 ES cells were aggregated with C57BL/6J x DBF1 eight-cell stage embryos in a hole on a plastic dish and cultured overnight. Then the well-formed blastocysts were transferred into the uterus of pseudopregnant female mice. Next, the male chimera mice were bred with C57BL/6J female mice, and germline transmission was checked by agouti coat color. Mice heterozygous for the mU50 mutation were crossed with C57BL/6-Tg(CAG-cre) mice to remove the *Neo*^{r} cassette flanked by loxP sites from the mU50 targeted locus [21]. The mice obtained were then backcrossed to the C57BL/6J genetic background for at least six generations. We used sixth generation mutant mice for most of the experiments and 10th generation for microarray and gene expression analyses.

Animals and Cells

Heterozygous mice were interbred or bred to C57BL/6J mice. All breeding was performed in a conditioned room (25°C, 60% humidity, and a 12:12 hour light-dark cycle) at the animal facility of Nippon Dental University, Tokyo, Japan.

A dissected spleen was gently ground by two slide-glasses and collected into a test tube with Hanks' balanced salt solution (HBSS; Invitrogen, USA). The cell pellet of the splenocytes was treated with 4 ml of ACK lysing buffer (Lonza, Germany) for 5 min to lyse out the erythrocytes. After several washings of the cells with HBSS, FITC-conjugated anti-CD45R/B220 antibody (BD Biosciences, USA) was added and reacted for 15 min on ice. Non-reacted antibody was washed out with HBSS, and then the cells were reacted with anti-FITC antibody-coupled magnetic beads (Miltenyi Biotec, USA) for 10 min. After rinsing twice, B-cells were separated using a LS+MACS separation column (Myltenyi Biotec).

Northern Blot Analysis

Total RNA was purified from mouse organs or isolated cells using ISOGEN reagent (Nippongene, Japan) according to the manufacturer's instructions. In brief, 10–20 μg of total RNA were denatured for 3 min at 95°C in 1×RNA buffer (49% formamide, 0.02% SDS, and 0.015% bromophenol blue) and separated on a denaturing gel (10% polyacrylamide (3.3% cross-linker), 7 M urea, and 1×TBE). Electrophoresis was performed at 12 W. Transfer onto a Hybond-N+ membrane (GE Biosciences, USA) was performed by electroblotting using a semidry blotting apparatus (TransblotSD, Bio-Rad, USA) at 2 mA/cm^2 for 35 min in 0.5×TBE. RNA was immobilized onto the membrane by UV cross-linking with 120 mJ in a UV Stratalinker (Stratagene, USA). An oligonucleotide probe was 5′-labeled with [γ-^{32}P]-ATP using T4 polynucleotide kinase (Promega, USA). Hybridization was carried out at 42°C in hybridization buffer (1 M sodium phosphate (pH 6.2) and 7% (w/v) SDS) for 16 h. Blotted membranes were washed twice for 10 min at 25°C in washing solution I (2×SSC, 0.1% (w/v) SDS) followed by a second washing step for 10 min with washing solution II (0.1×SSC, 0.1% (w/v) SDS). Membranes were exposed to a storage phosphor screen (Amersham) for 10–16 h and were scanned using a Typhoon image analyzer system (GE Biosciences). An oligonucleotide probe (5′-ATCTCAGAAGCCAGATCCGT-3′), which is complementary to the 3′-side of mU50 snoRNA sequence, was designed to hybridize all three mU50 snoRNA variants (Fig. 1B), and the oligonucleotide probe (5′-TCCTGCAATTCACATTAATTCTCGCAGCTAGC-3′), which is complementary to 5.8S rRNA, was used as the loading control. Densitometry was performed using ImageJ 1.45 (http://rsbweb.nih.gov/ij/).

Primer Extension Assay

Ten micrograms of total RNA with 0.5 pmol oligodeoxynucleotide primer that was conjugated with either AlexaFluor®488 or fluorescein (FAM) was heat denatured for 1 min at 95°C. Following a 10 min hybridization step at 43°C, reverse transcription was carried out in a buffer containing 200 units of M-MLV reverse transcriptase (Promega, USA) in the presence of either 1 mM dNTP or 0.004 mM dNTP. For the sequencing reactions, dideoxynucleotides were added to a final concentration of 0.06 mM. cDNA products were ethanol precipitated and primer extension products were resolved on a denaturing gel (6% polyacrylamide and 8 M urea) and visualized by scanning using a Typhoon Analyzer (Amersham). For sequencing ladders, a control rRNA gene sequence was obtained by PCR amplification of C57BL/6J genomic DNA with specific primers for the U50-sites (from 2537 bp to 2662 bp of the 28S rRNA gene), and the PCR product was cloned into a TA vector (Promega, USA). The primers that were used are listed in Table S2.

Real-time qPCR

RNA samples were treated with DNase I (Invitrogen), and then converted to cDNA using an oligo-dT primer and the SuperScript® First-strand synthesis system for RT-PCR (Invitrogen). qPCR was carried out using TaqMan® gene expression assay (ABI Inc., USA) and SYBR Green I® PCR Master Mix (ABI) with a Prism 7000 Real-time PCR System (ABI). Three technical replicates were run per sample. For the SYBR-based qPCR analysis, we tried several sets of PCR primers for each gene. The efficiency of each primer set was tested with serial dilutions of cDNA, and the combination of primers that yielded the best single amplified product was selected by checking for a single sharp peak in the dissociation curve of each product. The cycle threshold value (Ct) of each target gene was normalized relative to the reference genes (see below). All primer sets, except those for the TaqMan® assays, were designed using Primer3 via the NCBI webpage (http://www.ncbi.nlm.nih.gov/tools/primer-blast/) and are listed in Table S2.

To select appropriate reference genes for the survey of gene expression in various organs, we used the RefGenes tool from the Genevestigator platform [44] and selected the three top-ranking genes, *Tbc1d25*, *Bud13*, and *Krt81* (Fig. S5A). Microarray analysis confirmed that these genes were expressed equally in wild-type and $\Delta mU50_{(HG\text{-}b)}$ mice and that their signal intensities were at adequate levels but not as high as the signal intensity of the housekeeping *Actb* gene (Fig. S5B). We failed to obtain optimal amplification conditions for *Krt81*, but qPCR analyses showed that both *Tbc1d25* and *Bud13* yielded comparable expression levels (a reciprocal number of Ct value) among the eight organs analyzed (Fig. S5C). Based on these findings, we used *Tbc1d25* as a reference in all the qPCR analyses in this study.

PCR-SSCP

The cDNA library was constructed using a miScript system (QIAGEN, Germany) according to the manufacturer's instruction. Control plasmids containing individual mU50 variants were cloned into a pGEM-T easy vector (Promega). PCR primers for the mU50 sequence (forward, 5′-TCTATGATGATCCTATCCCG-3′; reverse, 5′-ATCTCAGAAGCCAGATCCGT-3′) were labeled with either AlexaFluor®647 or 6-carboxyfluorescein (6-FAM) at the 5′-ends. In the PCR reaction, 2 ng of template cDNA was used and amplified for 30 cycles. The PCR product was diluted to 1:125 with a loading buffer (96% deionized formamide containing 10 mM EDTA, 0.01% bromophenol blue), denatured at 95°C for 10 min, and applied to an acrylamide sequencing gel (10% native PAGE (aa:bis = 19:1) in 1×TBE). The gels were run at 1000 V (25V/cm) for 190 min at 22°C and scanned using a Typhoon scanner (GE Biosciences).

DNA Microarray

Microarray analysis was performed at the core facility of Cell Innovator Inc. (Fukuoka, Japan). Total RNA from splenic B-cells (23 weeks old; three samples per genotype) was purified with RNeasy Micro kit (QIAGEN). The quality of the RNA was assessed by monitoring the absorbance at 260 and 280 nm and rRNA fragmentation was measured using a Bioanalyzer (Agilent Technologies, USA). Concentrations of purified RNA samples were determined using a Nanodrop spectrophotometer (ND-1000; Thermo Scientific, USA) and equal amounts of the three RNA samples were mixed. cRNA was hybridized to a GeneChip® Microarray (Mouse Expression 430 2.0 Array, Affymetrix, USA) containing 45,101 probes that cover more than 20,000 mouse genes. The expression value and detection calls were computed from the raw data following the procedures outlined for the Affymetrix Microarray Suite software version 5.0. A complete gene list of the microarray analyses was built using GeneSpring software version 7.3.1 (Silicon Genetics Inc., USA). Because arranged immunoglobulin (Ig) genes could not be distinguished in the mixed samples, we omitted the probes for Ig genes from the analysis.

Data Deposition

The microarray data have been deposited and are available online in the Gene Expression Omnibus (GEO) database (http://www.ncbi.nlm.nih.gov/geo/) under the accession number GSE41164.

Supporting Information

Figure S1 Structural bases of mU50 snoRNA. (A) Computer-assisted prediction of the secondary structure of mU50 snoRNA variants. The k-turn structure that might possibly be formed by box C and D motifs was not taken into account for the prediction. Note that the all three variants exhibit the identical structure at the most stable energy states. (B) Sequence similarity among human and mouse U50 snoRNAs. Human U50A and U50B snoRNAs (formerly U50 and U50' in [17]) are compared with the mU50 snoRNA sequence. Conserved box motifs are indicated by rectangles. Antisense elements to 28S rRNA are indicated by broken lines. The four U residues in the U50A snoRNA (shown in red and underscored) are where a genomic TT-deletion has been reported in prostate and breast cancers [18,19]. (C) Schematic representation and nucleotide sequences of the mU50 snoRNA target sites (in orange) on the rRNA gene in five organisms. The segments down-stream of the mU50-sites (gray rectangles) are variable having expanded in size through insertions and/or duplications during the evolutionary process. A further comparative genomic data analysis indicated that the U50-sites are highly conserved from archaea to vertebrate. Referring to a previous report of the *T. thermophilus* 23S rRNA structure [32], the conserved site for the mU50-sites is subject to form the loop 62 which participates in the formation of the inter-subunit bridge. (PDF)

Figure S2 Nucleotide sequences of the modified *mU50HG-b* gene in comparison with the original sequence in wild-type. The sequence starts from the intron 3 which contains an mU50 snoRNA sequence (upstream) through the intron 4 where another mU50 sequence (downstream) resides. mU50 snoRNA and exon sequences are shown in blue and black

background, respectively. Nucleotides unaltered upon the recombination are connected with asterisks. The upstream mU50 sequence is completely replaced with a non-coding sequence derived from pBluescript II plasmid, and the downstream mU50 sequence is replaced with residual nucleotides of the loxP-*Neo*^{r}-loxP cassette after the Cre-lox recombination. Note that the sizes of the modified introns are identical to those of wild-type.
(PDF)

Figure S3 Phenotypes of the mU50-deficient animals. (A) Weight gain of female and male $\Delta mU50_{(HG\text{-}b)}$ and wild-type mice (n = 14 per genotype). A plot of $\Delta mU50_{(HG\text{-}b)}$ mice was always lower than that of the wild-type mice throughout the observation period, although this difference was not statistically significant. Error bars = 1. S.D. (standard deviation) (B) Average tissue weight (% body-weight) in wild-type and $\Delta mU50_{(HG\text{-}b)}$ mutant mice at 10 weeks after birth (n = 7 per genotype). Although some organs such as heart, liver, and testis of $\Delta mU50_{(HG\text{-}b)}$ mice were lighter than the same organs in wild-type, no prominent differences were found in their morphology and histology (data not shown). Error bars = 1 S.D. *P<0.05. (C) Age-associated changes in the number of peripheral lymphocytes (n = 4 per genotype) in $\Delta mU50_{(HG\text{-}b)}$ and wild-type mice. Fitted curves for $\Delta mU50_{(HG\text{-}b)}$ (broken line) and wild-type (solid line) are indicated. (D) Proliferation activity of splenocytes *in vitro*. For cell culture, 2×10^5 of isolated splenocytes from individual genotypes were grown on 6-well plates (BD Falcon, USA) in the presence of 1.0 μg/ml of lipopolysaccharides (Sigma, USA) as a stimulus. The numbers of cells were counted with a hemocytometer. The number of cells 24 h after inoculation was designated as 100%. Error bars = 1 S.D. from three independent assays.
(PDF)

Figure S4 Representative data of qPCR validation of relative gene expression in splenocytes between wild-type and $\Delta mU50_{(HG\text{-}b)}$ mice. The threshold value was normalized by the beta-actin gene (*Actb*) according to the ΔΔCt method. Error bars = 1 S.D. for three biological replicates. *P<0.05; WT: wild-type; Δ: $\Delta mU50_{(HG\text{-}b)}$ mice.
(PDF)

Figure S5 Selection of qPCR reference genes for assessment of organ-dependent gene expression patterns. (A) A result view of RefGenes platform [44] on inquiry for appropriate reference genes for qPCR survey to eight organs. The 3 top-ranking candidates were *Tbc1d25*, *Bud13*, and *Krt81*. (B) Comparable expression levels of the candidate genes obtained from microarray analysis of splenic B-cells in wild-type and $\Delta mU50_{(HG\text{-}b)}$ mice. (C) TaqMan®-based qPCR analyses of the candidate genes in various organs of wild-type mice. The expression levels (a reciprocal number of Ct value) of reference genes among eight organs are compared. Note that both *Tbc1d25* and *Bud13* showed less inter-organ variations in their expression levels as compared to those of *Actb*.
(PDF)

Figure S6 Comparative genomic analyses of human and mouse mU50 host-gene promoter sites. (A) The phylogenetic tree was constructed based on the promoter sequences (from −2,000 bp behind 5′TOP transcription start site to +500 bp) of these U50 snoRNA host-genes using VISTA tools for comparative genomics that is provided by Lawrence Berkeley National Laboratory (http://genome.lbl.gov/vista/index.shtml). The results support the closest promoter sequence of *mU50HG-b* to human *U50HG*. (B) Conservation of promoter sequences among human and mouse U50 host-genes. Highly conserved loci (>70% similarity) with human *U50HG* are shown in pink.
(PDF)

Table S1 Anomalies detected in age-matched wild-type and $\Delta mU50_{(HG\text{-}b)}$ mice. Age-matched mice that were euthanized or had died were examined pathologically (n = 40 per genotype).
(DOC)

Table S2 List of PCR primers used in this study.
(DOC)

Acknowledgments

We thank to Drs. Hitoshi Satoh and Tetsuro Hirose for valuable discussion on the generation of the mouse model.

Author Contributions

Conceived and designed the experiments: Y. Soeno MA S. Kakuta RTF SM TA. Performed the experiments: Y. Soeno KF TK YT Y. Shimazu KS S. Kubo. Analyzed the data: Y. Soeno MA S. Kakuta KS TA. Contributed reagents/materials/analysis tools: S. Kubo YI YN SM. Wrote the paper: Y. Soeno TA.

References

1. Matera AG, Terns RM, Terns MP (2007) Non-coding RNAs: lessons from the small nuclear and small nucleolar RNAs. Nat Rev Mol Cell Biol 8: 209–220.
2. Williams GT, Farzaneh F (2012) Are snoRNAs and snoRNA host genes new players in cancer? Nat Rev Cancer 12: 84–88.
3. Kiss-Laszlo Z, Henry Y, Bachellerie JP (1996) Site-specific ribose methylation of preribosomal RNA: a novel function for small nucleolar RNAs. Cell 85: 1077–1088.
4. Kiss-Laszlo Z, Henry Y, Kiss T (1998) Sequence and structural elements of methylation guide snoRNAs essential for site-specific ribose methylation of pre-rRNA. EMBO J 17: 797–807.
5. Bachellerie JP, Cavaillé J, Hüttenhofer A (2002) The expanding snoRNA world. Biochimie 84: 775–790.
6. Hüttenhofer A, Brosius J, Bachellerie JP (2002) RNomics: identification and function of small, non-messenger RNAs. Curr Opin Chem Biol 6: 835–843.
7. Filipowicz W, Pogacic V (2002) Biogenesis of small nucleolar ribonucleoproteins. Curr Opin Cell Biol 14: 319–327.
8. Kiss T (2002) Small nucleolar RNAs: an abundant group of noncoding RNAs with diverse cellular functions. Cell 109: 145–148.
9. Dieci G, Preti M, Montanini B (2009) Eukaryotic snoRNAs: A paradigm for gene expression flexibility. Genomics 94: 83–88.
10. Richard P, Kiss AM, Darzacq X, Kiss T (2006) Cotranscriptional recognition of human intronic box H/ACA snoRNAs occurs in a splicing-independent manner. Mol Cell Biol 26: 2540–2549.
11. Tycowski KT, Shu MD, Steitz JA (1996) A mammalian gene with introns instead of exons generating stable RNA products. Nature 379: 464–466.
12. Pelczar P, Filipowicz W (1998) The host gene for intronic U17 small nucleolar RNAs in mammals has no protein-coding potential and is a member of the 5′-terminal oligopyrimidine gene family. Mol Cell Biol 18: 4509–4518.
13. Smith CM, Steitz JA (1998) Classification of gas5 as a multi-small-nucleolar-RNA (snoRNA) host gene and a member of the 5′-terminal oligopyrimidine gene family reveals common features of snoRNA host genes. Mol Cell Biol 18: 6897–6909.
14. Lowe TM, Eddy SR (1999) A computational screen for methylation guide snoRNAs in yeast. Science 283: 1168–1171.
15. Esguerra J, Warringer J, Blomberg A (2008) Functional importance of individual rRNA 2′-O-ribose methylations revealed by high-resolution phenotyping. RNA 14: 649–656.
16. Esteller M (2011) Non-coding RNAs in human disease. Nat Rev Genet 12: 861–874.
17. Tanaka R, Satoh H, Moriyama M, Satoh K, Morishita Y, et al. (2000) Intronic U50 small-nucleolar-RNA (snoRNA) host gene of no protein-coding potential is mapped at the chromosome breakpoint t(3;6)(q27;q15) of human B-cell lymphoma. Genes Cells 5: 277–287.
18. Dong X-Y, Rodriguez C, Guo P, Sun X, Talbot JT, et al. (2008) SnoRNA U50 is a candidate tumor-suppressor gene at 6q14.3 with a mutation associated with clinically significant prostate cancer. Hum Mol Genet 17: 1031–1042.

19. Dong X-Y, Guo P, Boyd J, Sun X, Li Q, et al. (2009) Implication of snoRNA U50 in human breast cancer. J Genet Genomics 36: 447–454.
20. Tanaka-Fujita R, Soeno Y, Satoh H, Nakamura Y, Mori S (2007) Human and mouse protein-noncoding snoRNA host genes with dissimilar nucleotide sequences show chromosomal synteny. RNA 13: 811–816.
21. Sakai K, Miyazaki J (1997) A transgenic mouse line that retains Cre recombinase activity in mature oocytes irrespective of the cre transgene transmission. Biochem Biophys Res Commun 237: 318–324.
22. Fernandez PC, Frank SR, Wang L, Schroeder M, Liu S, et al. (2003) Genomic targets of the human c-Myc protein. Gene Dev 17: 1115–1129.
23. Skryabin BV, Gubar LV, Seeger B, Pfeiffer J, Handel S, et al. (2007) Deletion of the MBII-85 snoRNA gene cluster in mice results in postnatal growth retardation. PLoS Genet 3: e235.
24. Ding F, Li HH, Zhang S, Solomon NM, Camper SA, et al. (2008) SnoRNA Snord116 (Pwcr1/MBII-85) deletion causes growth deficiency and hyperphagia in mice. PLoS ONE 3: e1709.
25. Cohen DI, Steinberg AD, Paul WE, Davis MM (1985) Expression of an X-linked gene family (XLR) in late-stage B cells and its alteration by the xid mutation. Nature 314: 372–374.
26. Nakajima M, Miyamoto Y, Ikegawa S (2011) Cloning and characterization of the osteoarthritis-associated gene DVWA. J Bone Miner Metab 29: 300–308.
27. Vitali P, Basyuk E, Le Meur E, Bertrand E, Muscatelli F, et al. (2005) ADAR2-mediated editing of RNA substrates in the nucleolus is inhibited by C/D small nucleolar RNAs. J Cell Biol 169: 745–753.
28. Kishore S, Stamm S (2006) The snoRNA HBII-52 regulates alternative splicing of the serotonin receptor 2C. Science 311: 230–232.
29. Schoemaker RJW, Gultyaev AP (2006) Computer simulation of chaperone effects of archaeal C/D box sRNA binding on rRNA folding. Nucleic Acids Res 34: 2015–2026.
30. Vos MJ, Hageman J, Carra S, Kampinga HH (2008) Structural and functional diversities between members of the human HSPB, HSPH, HSPA, and DNAJ chaperone families. Biochemistry 47: 7001–7011.
31. Baxter-Roshek JL, Petrov AN, Dinman JD (2007) Optimization of ribosome structure and function by rRNA base modification. PLoS ONE 2: e174. doi:10.1371/journal.pone.0000174.
32. Yusupov MM, YusupovaGZ, Baucom A, Lieberman K, Earnest TN, et al. (2001) Crystal structure of the ribosome at 5.5 Å resolution. Science 292: 883–896.
33. Decatur WA, Fournier MJ (2002) rRNA modifications and ribosome function. Trends Biochem Sci 27: 344–351.
34. Brimacombe R, Mitchell P, Osswald M, Stade K, Bochkariov D (1993) Clustering of modified nucleotides at the functional center of bacterial ribosomal RNA. FASEB J 7: 161–167.
35. Maquat LE (2004) Nonsense-mediated mRNA decay: splicing, translation and mRNP dynamics. Nat Rev Mol Cell Biol 5: 89–99.
36. Makarova JA, Kramerov DA (2005) Noncoding RNA of U87 host gene is associated with ribosomes and is relatively resistant to nonsense-mediated decay. Gene 363: 51–60.
37. Ender C, Krek A, Friedländer MR, Beitzinger M, Weinmann L, et al. (2008) A human snoRNA with microRNA-like functions. Mol Cell 32: 519–528.
38. Taft RJ, Glazov EA, Lassmann T, Hayashizaki Y, Carninci P, et al. (2009) Small RNAs derived from snoRNAs. RNA 15: 1233–1240.
39. Brameier M, Herwig A, Reinhardt R, Walter L, Gruber J (2010) Human box C/D snoRNAs with miRNA like functions: expanding the range of regulatory RNAs. Nucleic Acids Res 39: 675–686.
40. Mourtada-Maarabouni M, Pickard MR, Hedge VL, Farzaneh F, Williams GT (2009) GAS5, a non-protein-coding RNA, controls apoptosis and is downregulated in breast cancer. Oncogene 28: 195–208.
41. Mourtada-Maarabouni M, Hasan AM, Farzaneh F, Williams GT (2010) Inhibition of human T-cell proliferation by mammalian target of rapamycin (mTOR) antagonists requires noncoding RNA growth-arrest-specific transcript 5 (GAS5). Mol Pharmacol 78: 19–28.
42. Askarian-Amiri ME, Crawford J, French JD, Smart CE, Smith MA, et al. (2011) SNORD-host RNA Zfas1 is a regulator of mammary development and a potential marker for breast cancer. RNA 17: 878–891.
43. Asano M, Furukawa K, Kido M, Matsumoto S, Umesaki Y, et al. (1997) Growth retardation and early death of b-1,4-galactosyltransferase knockout mice with augmented proliferation and abnormal differentiation of epithelial cells. EMBO J 16: 1850–1857.
44. Hruz T, Wyss M, Docquier M, Pfaffl MW, Masanetz S, et al. (2011) RefGenes: identification of reliable and condition specific reference genes for RT-qPCR data normalization. BMC Genomics 12: 156. doi:10.1186/1471-2164-12-156.
45. Hirose T, Steitz J (2001) Position within the host intron is critical for efficient processing of box C/D snoRNAs in mammalian cells. Proc Natl Acad Sci USA 98: 12914–12919.

Hepatology Research

Hepatology Research 2014; 44: 460–473 doi: 10.1111/hepr.12140

Original Article

Cilostazol attenuates hepatic stellate cell activation and protects mice against carbon tetrachloride-induced liver fibrosis

Shunichi Saito,[1] Koichiro Hata,[1] Keiko Iwaisako,[1,3] Atsuko Yanagida,[1] Masatoshi Takeiri,[2] Hirokazu Tanaka,[1] Shoichi Kageyama,[1] Hirofumi Hirao,[1] Kazuo Ikeda,[3] Masataka Asagiri[2] and Shinji Uemoto[1]

[1]Department of Surgery, Division of Hepato-Pancreato-Biliary Surgery and Transplantation, and [2]Innovation Center for Immunoregulation and Therapeutics, Graduate School of Medicine, Kyoto University, Kyoto, and [3]Department of Anatomy and Regenerative Biology, Graduate School of Medicine, Osaka City University, Osaka, Japan

Aim: Liver fibrosis is a common pathway leading to cirrhosis. Cilostazol, a clinically available oral phosphodiesterase-3 inhibitor, has been shown to have antifibrotic potential in experimental non-alcoholic fatty liver disease. However, the detailed mechanisms of the antifibrotic effect and its efficacy in a different experimental model remain elusive.

Methods: Male C57BL/6J mice were assigned to five groups: mice fed a normal diet (groups 1 and 2); 0.1% or 0.3% cilostazol-containing diet (groups 3 and 4, respectively); and 0.125% clopidogrel-containing diet (group 5). Two weeks after feeding, groups 2–5 were intraperitoneally administered carbon tetrachloride (CCl_4) twice a week for 6 weeks, while group 1 was treated with the vehicle alone. To investigate the effects of cilostazol on hepatic cells, *in vitro* studies were conducted using primary hepatic stellate cells (HSC), Kupffer cells and hepatocytes with cilostazol supplementation.

Results: Sirius red staining revealed that groups 3 and 4 exhibited a lesser fibrotic area (2.49 ± 0.43% and 2.31 ± 0.30%, respectively) than group 2 (3.17 ± 0.67%, $P < 0.05$ and $P < 0.001$, respectively). *In vitro* studies showed cilostazol dose-dependently suppressed HSC activation (assessed by morphological change, cell proliferation, and the expression of HSC activation markers), suggesting the therapeutic effect of cilostazol is mediated by its direct action on HSC.

Conclusion: Cilostazol could alleviate CCl_4-induced hepatic fibrogenesis *in vivo*, presumably due, at least partly, to its direct effect to suppress HSC activation. Given its clinical availability and safety, it may be a novel therapeutic intervention for chronic liver diseases.

Key words: carbon tetrachloride, cilostazol, hepatic stellate cells, liver fibrosis, phosphodiesterase-3 inhibitor, platelet-derived growth factor

Correspondence: Dr Koichiro Hata, Department of Surgery, Division of Hepato-Pancreato-Biliary Surgery and Transplantation, Graduate School of Medicine, Kyoto University, Kyoto 606-8507, Japan.
Email: khata@kuhp.kyoto-u.ac.jp; Dr Masataka Asagiri, Innovation Center for Immunoregulation and Therapeutics, Graduate School of Medicine, Kyoto University, Kyoto 606-8501, Japan.
Email: masa-asagiri@umin.org

Conflict of interest: Drs Hata and Uemoto receive a grant from Otsuka Pharma. Dr Asagiri receives a grant from the AK Project (between Astellas Pharma and Kyoto University). However, the study was designed, conducted, analyzed, and reported independently of the funding agencies and pharmaceutical companies, although cilostazol was supplied by Otsuka Pharmaceutical. No other potential conflict of interest relevant to this article was reported.
Received 17 August 2012; revision 8 April 2013; accepted 15 April 2013.

INTRODUCTION

LIVER FIBROSIS, A precursor to cirrhosis, is a common consequence of almost all types of chronic liver injuries, including viral, alcoholic, autoimmune, metabolic and drug-induced liver diseases.[1] Fibrosis results from excessive accumulation of extracellular matrix (ECM) components, such as collagen type I. Left untreated, fibrosis can progress to liver cirrhosis and ultimately lead to organ failure and death. The activation of hepatic stellate cells (HSC) in response to liver injury is considered to be an essential event underlying hepatic fibrogenesis.[2–4] The activation of HSC refers to the trans-differentiation of quiescent HSC into proliferative and contractile myofibroblast-like cells. These activated HSC

secrete excess ECM proteins and contribute to the development of hepatic fibrosis. Several types of growth factors, cytokines, chemokines and their cognate receptors are associated with HSC activation. Among these, transforming growth factor (TGF)-β1 and platelet-derived growth factor (PDGF) are probably the most important.[5–7] HSC play a key role in liver fibrosis, thereby restraining the activation of HSC may attenuate liver fibrosis. Thus, numerous studies have attempted to suppress HSC activation in order to develop new treatment strategies for hepatic fibrosis.[8–11] Cilostazol (OPC-13013 [6-[4-[1-cyclohexyl-1H-tetrazol-5-yl]butoxy]-3,4-dihydro-2[1H]-quinolinone]) is a synthetic vasodilator and an antiplatelet agent. It was approved in 1988 in Japan for the treatment of symptoms related to occlusive peripheral arterial disease (Pletaal; Otsuka Pharmaceutical Co., Ltd., Tokyo, Japan) and subsequently in 1999 in the USA and in 2001 in the UK (Pletal; Otsuka America Pharmaceutical, Inc., Rockville, MD, USA and Otsuka Pharmaceutical Europe Ltd., Uxbridge, UK) for the treatment of intermittent claudication symptoms.[12–14] Over the past 20 years, it has been widely used as a potent inhibitor of platelet aggregation and thrombosis.[15–18] It has also been shown to inhibit PDGF secretion *in vitro*.[19] The antiplatelet activity of cilostazol is attributed to its inhibition of cyclic adenosine monophosphate (cAMP) phosphodiesterase (PDE). Recent studies have identified 11 different families of PDE. Of these, cilostazol selectively inhibits PDE3, which is predominantly expressed in platelets, vascular smooth muscle cells, cardiac myocytes and hepatic cells.[20,21] Recently, increased intracellular cAMP has been shown to inhibit HSC activation,[22–25] although little is known about the effect of cilostazol on liver fibrosis. Furthermore, cilostazol was shown to have an antifibrotic potential in experimental non-alcoholic fatty liver disease.[26] However, the precise mechanisms of the antifibrotic effect and its efficacy in a different experimental model are elusive. This study was designed to investigate the effect of cilostazol on carbon tetrachloride (CCl_4)-induced hepatic fibrogenesis in mice and to clarify its mechanism of action by pathological examination and analysis of primary cells derived from the mice.

METHODS

Animals

MALE C57BL/6J MICE aged 4 weeks were purchased from Japan SLC (Shizuoka, Japan). After an acclimation period of 7 days, the mice were randomly assigned to the five treatment groups ($n = 10$ per group) in a single-blinded fashion (Fig. 1). The mice were maintained on standard chow and allowed free access to food and water. The protocol for animal handling was reviewed and approved by the Animal Care and Use Committee of Kyoto University.

Mouse model of liver fibrosis

Two weeks after assignment to treatment groups, the mice were treated with CCl_4 (2 μL/g bodyweight diluted 1:4 in corn oil) by intraperitoneal (i.p.) injection twice a week for 6 weeks. The mice were sacrificed 4 days after the last injection.

Drugs and drug treatment

The antiplatelet drug cilostazol was a gift from Otsuka Pharma (Tokushima, Japan). Clopidogrel was purchased from Sanofi-Aventis (Tokyo, Japan). Each drug was administrated in standard pellet food (Oriental Bio Service, Kyoto, Japan) containing cilostazol (0.1% w/w), cilostazol (0.3% w/w) or clopidogrel (0.125% w/w). Oral treatment with cilostazol at 0.1% and 0.3% w/w, and clopidogrel at 0.125% w/w of chow is equivalent to the clinically used doses.[27–29] The alternative antiplatelet drug clopidogrel was used as a control. To raise and stabilize the plasma concentration of the drugs, the animals were pretreated with the drugs for 2 weeks. All animals were closely observed for 2 weeks after the dietary change, and then received CCl_4 injections for 6 weeks. The food intake and bodyweight changes were monitored throughout the experimental period for 8 weeks. Blood samples were collected from the inferior vena cava of the mice, and liver weights were recorded at death.

Histological examination and immunohistochemistry

For histological evaluation, the right lobe of the liver of each mouse was collected at death and fixed in 4% paraformaldehyde (PFA). In order to assess fibrosis, paraffin-embedded sections were stained with picrosirius red (Sigma, St Louis, MO, USA).[30] Expression levels of α-smooth muscle actin (α-SMA) and F4/80 were immunohistochemically determined in paraffin-embedded sections as described previously[31] using a monoclonal antimouse α-SMA antibody (1:300, clone: 1A4; Dako, Glostrup, Denmark) or anti-mouse F4/80 antibody (1:100, clone: BM8; eBioscience, San Diego, CA, USA), respectively.

Sirius red-positive areas, α-SMA-positive areas and F4/80-positive areas were quantified from 10 random ×100 fields from each animal ($n = 10$ per treatment

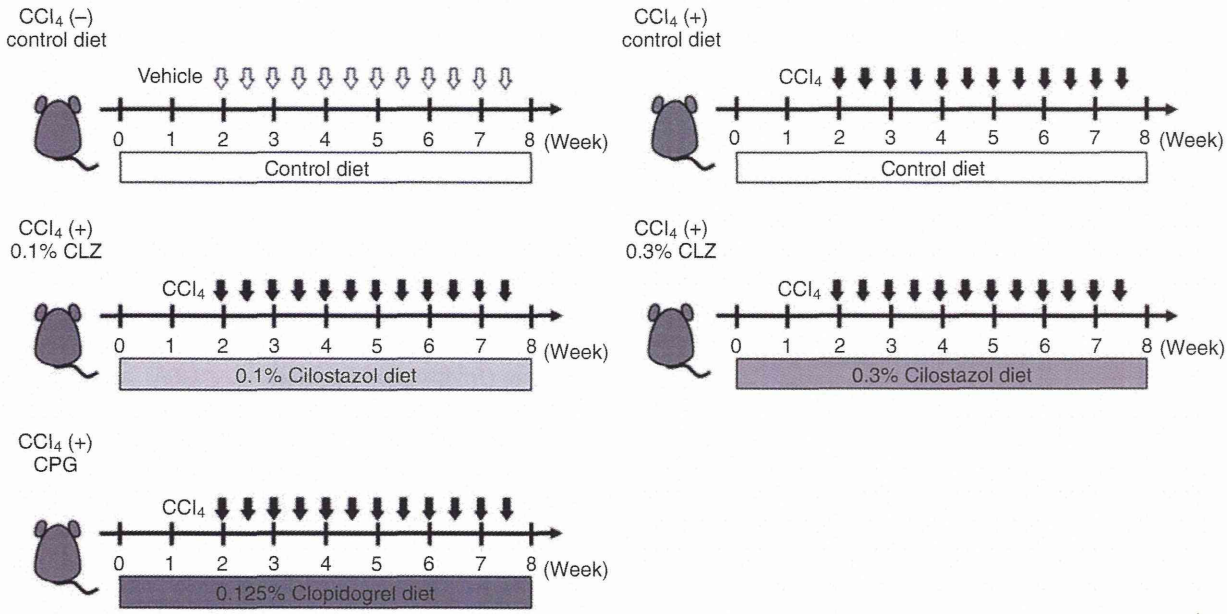

Figure 1 Experimental protocol. Male adult C57BL/6J mice were fed pelleted food containing 0.1% or 0.3% cilostazol or 0.125% clopidogrel, or fed a control diet. Liver fibrosis was induced by i.p. injection of CCl_4 twice a week for 6 weeks. Mice were killed 4 days after the last injection. CLZ, cilostazol; CPG, clopidogrel; CCl_4, carbon tetrachloride. ($n = 10$). ⇩, vehicle i.p.; ⬇, CCl_4, 0.5 μL/g bodyweight i.p.

group) using image processing software (BZ analyzer; Keyence, Osaka, Japan). Data are presented as the percentage area positively stained for Sirius red, α-SMA or F4/80.

Measurement of hepatic collagen content

For measurement of liver fibrosis, the specific amino acid of collagen type I, hydroxyproline, was quantified in liver tissue. The hepatic hydroxyproline content was measured as previously described.[32] In brief, liver tissue was homogenized in 900 μL of ice-cold distilled water. Subsequently, 125 μL of 50% trichloroacetic acid was added, and the homogenates were incubated on ice for 20 min. Precipitated pellets were hydrolyzed for 18 h at 110°C in 6 N HCl. After hydrolysis, the samples were filtered and neutralized with 10 N NaOH, and hydrolysates were oxidized with chloramine-T (Sigma) for 25 min at room temperature. The reaction mixture was then incubated in Ehrlich's perchloric acid solution at 65°C for 20 min and then cooled to room temperature. Sample absorbance was measured at 560 nm in duplicate. Purified hydroxyproline (Sigma) was used as a standard. The hydroxyproline content was expressed as nanograms of hydroxyproline per gram of liver.

Immunoblot analysis

For analysis of α-SMA protein expression, immunoblotting was performed with whole liver lysates (20 μg/lane) using standard techniques. Immunoblotting was performed using a polyclonal antigoat glyceraldehyde 3-phosphate dehydrogenase (GAPDH) antibody (1:200; #sc-20357; Santa Cruz Biotechnology, Santa Cruz, CA, USA) as an internal control, a polyclonal antirabbit α-SMA antibody (1:200; #ab-5694; Abcam, Cambridge, UK) and horseradish peroxidase-conjugated secondary antibodies (Santa Cruz Biotechnology) as described in the manufacturer's protocol.[33] Antibody staining was visualized with an enhanced chemiluminescence system (GE Healthcare Biosciences, Little Chalfont, UK) using Lumino-image analyzer (LAS-3000 mini; Fujifilm, Tokyo, Japan). Band density was quantified from digital images using ImageJ software.

Isolation and culture of hepatic cells

Primary HSC, Kupffer cells and hepatocytes were isolated from the mouse liver as described previously.[34–36] In brief, HSC and Kupffer cells were isolated from mice by two-step collagenase–pronase perfusion followed by three-layer discontinuous density gradient

centrifugation with 8.2% (w/v) and 14.5% (w/v) Nycodenz (Accurate Chemical and Scientific, Westbury, NY, USA) to obtain HSC and Kupffer cell fractions. HSC were collected between the 0% and 8.2% (w/v) layer. Kupffer cells were collected between the 8.2% and 14.5% (w/v) layers and purified by differential plating. HSC and Kupffer cells were cultured in Dulbecco's modified Eagle's medium (DMEM; Sigma) supplemented with 10% fetal bovine serum (FBS) and antibiotics. Hepatocytes were cultured in William's medium E supplemented with 10% FBS and antibiotics on the collagen-coated dish. Hepatic cells were cultured in a CO_2 incubator at 37°C.

Cilostazol treatment

Cilostazol was dissolved in dimethylsulfoxide and diluted in DMEM supplemented with 10% FBS and antibiotics. Complete medium containing final concentration of 0 μM (control), 5 μM and 15 μM cilostazol was added to cultures 1 day after isolation.

Measurement of Intracellular cAMP

The intracellular cAMP level was measured as described previously[37] using the cAMP-Glo max assay kit (Promega, Madison, WI, USA). Briefly, 1×10^4 cells were seeded in a 96-well plate with or without cilostazol in culture medium containing 10% FBS and incubated at 37°C for 24 h. The cAMP detecting solution was added to each well and incubated at room temperature for 20 min. The Kinase-Glo reagent was added to each well. The plate was shaken for 1 min at room temperature and incubated at room temperature for 10 min. Finally, the luminescent signal was measured by a plate reader (Arvo; Perkin-Elmer, Waltham, MA, USA).

Time-lapse recording and cell counting

For the observation of morphological changes, HSC were placed in a Lab-Tek plastic four-well chamber slide (Nunc, Naperville, IL, USA) and maintained at 37°C in 10% CO_2. Time-lapse images were taken using an inverted microscope (BZ9000; Keyence, Osaka, Japan) over 6 days following cilostazol treatment. Cells were counted in four random ×200 fields on each chamber using BZ analyzer image processing software.

Cytochemical analysis

Primary HSC in each chamber were fixed in 10% formalin/PBS for 10 min blocked with Dako Protein Block (#X0909; Dako, Glostrup, Denmark) for 1 h, incubated overnight with a polyclonal antimouse α-SMA antibody (1:200; #A2524, Sigma) in a blocking solution, washed with PBS, and incubated with Alexa Flour 594 goat antimouse immunoglobulin G (1:600; #A-11005; Invitrogen, San Diego, CA, USA) secondary antibody and 4′,6′-diamidino-2-phenylindole dihydrochloride (DAPI) nuclear stain for 1 h. Finally, HSC were washed and observed with an inverted fluorescence microscope, BZ9000 (Keyence).

Reverse-transcriptase quantitative polymerase chain reaction (RT–qPCR)

For gene expression analysis, total RNA was extracted from liver tissue, HSC or Kupffer cells using TRIZOL reagent (Invitrogen, Carlsbad, CA, USA) according to the manufacturer's protocol. DNase-treated RNA was reverse transcribed using the Omniscript RT Kit (Qiagen, Hilden, Germany) according to the manufacturer's protocol. RT-qPCR was performed for 55 cycles of 15 s at 95°C and 60 s at 60°C using SYBR Green I Kits for the LightCycler 480 instrument (Roche Diagnostics, Mannheim, Germany). The relative abundance of target genes was calculated using a standard curve normalized to α-tubulin or 18S. Probes and primers for α-SMA (NM_007392), collagen α1 (I) (NM_007742), PDGF-B (NM_011057), PDGF receptor (PDGFR)-β (NM_008809), TGF-β1 (NM_011577), TGF-βR1 (NM_009370), tumor necrosis factor (TNF)-α (NM_013693), interleukin (IL)-1β (NM_008361), monocyte chemotactic protein (MCP)1 (NM_011333), F4/80 (NM_010130), 18S (NR_003278) and α-tubulin (NM_011653) were designed by and purchased from Life Technologies (Carlsbad, CA, USA).

Statistical analysis

Results are reported as mean ± 95% confidence intervals (CI). Statistical comparisons were made using Student *t*-test or two- or one-way ANOVA followed by Bonferroni's post-hoc test. $P < 0.05$ was considered to be significant.

RESULTS

Cilostazol alleviated fibrous change in the liver

IN ORDER TO validate the antifibrotic efficacy of cilostazol, we utilized a widely used experimental mouse model of liver fibrosis induced by CCl_4 injections (twice a week for 6 weeks; Fig. 1). Based on the pharmacokinetic data of the plasma concentration of the drugs, 0.1% and 0.3% cilostazol and 0.125% clopidogrel were used as clinically equivalent doses. Collagen deposition, a marker for liver fibrosis, was assessed by Sirius red

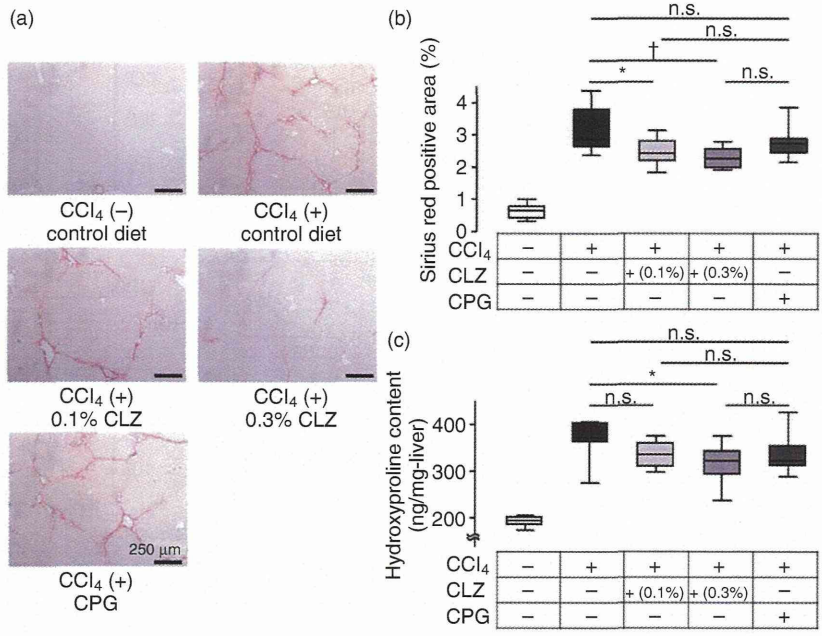

Figure 2 Cilostazol alleviated fibrous changes in the liver. (a) Sirius red staining of liver sections in each group. CCl_4 treatment for 6 weeks remarkably increased the fibrotic area. CCl_4-treated liver in the control or clopidogrel-administrated group showed bridging fibrosis. Cilostazol decreased the fibrotic area among CCl_4-treated mice (original magnification ×100). (b) Quantification of liver fibrosis area stained by Sirius red. CCl_4-induced fibrous areas in the 0.1% or 0.3% cilostazol-administrated groups were significantly decreased compared with that in the control group. (c) Hydroxyproline assay was performed to measure the total collagen content. Administration with 0.3% cilostazol reduced tissue hydroxyproline levels compared with control. The box plots present the median and 25th–75th percentiles. Upper and lower lines represent the minimum and maximum values ($n = 10$). *$P < 0.05$; †$P < 0.001$ vs CCl_4-treated control. CCl_4, carbon tetrachloride; CLZ, cilostazol; CPG, clopidogrel.

staining (Fig. 2a). Sirius red staining of the liver in the 0.1% and 0.3% cilostazol-administrated groups (2.49%; 95% CI = 2.18–2.80; and 2.31%; 95% CI = 2.10–2.52) was significantly lower than in the control group (3.17%; 95% CI = 2.70–3.65; $P < 0.05$ and $P < 0.001$, respectively), however, clopidogrel had no effect (Fig. 2a,b). This was reflected by hydroxyproline content, which was significantly reduced in the 0.3% cilostazol-administrated group (317 ng/mg liver; 95% CI = 289–346) compared with that in the control group (371 ng/mg liver; 95% CI = 344–398; $P < 0.001$; Fig. 2c). Thus, p.o. administration of cilostazol reduces hepatic fibrogenesis at clinical doses. During the 8-week experimental duration, no significant difference in bodyweight change or peripheral platelet count was observed among treatment groups (Fig. 3a,b), indicating minimal toxicity of the drugs. Moreover, there was no apparent difference in CCl_4-induced hepatocyte damage among the groups, as assessed by peripheral blood aspartate aminotransferase and alanine aminotransferase levels (Fig. 3c,d) and hematoxylin–eosin staining (Fig. 3e). We also observed no morphological change in cultured primary hepatocytes supplemented with cilostazol (Fig. 3f).

Cilostazol attenuated the activation of HSC in the liver

Chronic liver injury can lead to unrestrained HSC activation, resulting in excessive production of extracellular matrices and hepatic fibrosis. Thus, we assessed the activation status of HSC in the liver, by immunohistochemical staining of α-SMA, a marker of HSC activation (Fig. 4a). Similar to the Sirius red staining data, the α-SMA positive area in the liver of the 0.1% (4.16%; 95% CI = 3.17–5.15) and 0.3% (2.61%; 95% CI = 2.17–3.05) cilostazol-administrated groups was clearly reduced in a dose-dependent manner compared with the control group (7.13%; 95% CI = 4.10–10.2; $P < 0.05$ and $P < 0.001$, respectively; Fig. 4b) and clopidogrel-administrated animals. This result was also reflected by immunoblotting experiments in which α-SMA protein expression was significantly reduced in